ACS APPLIED MATERIALS & INTERFACES

Research Article

www.acsami.org

17β-Estradiol-Loaded PEGlyated Upconversion Nanoparticles as a Bone-Targeted Drug Nanocarrier

Yan Hu,[†] Jiachang Li,[‡] Xingjun Zhu,[‡] Yuhao Li,[‡] Shuang Zhang,[†] Xiaojing Chen,[†] Yanhong Gao,*[,†] and Fuyou Li*[,‡]

[†]Department of Geriatrics, Xinhua Hospital of Shanghai Jiaotong University, School of Medicine, Shanghai 200092, PR China

[‡]Department of Chemistry & Institutes of Biomedical Sciences & Advanced Materials Laboratory, Fudan University, 220 Handan Road, Shanghai 200433, PR China

Supporting Information

ABSTRACT: Hormone replacement therapy (HRT) plays an important role in the treatment and prevention of osteoporosis. Here, 17β-estradiol (E2)-loaded PEGlyated upconversion nanoparticles (E2-UCNP@pPEG) were synthesized that retained E2 bioactivity and improved delivery efficiency over a relatively long time-period. E2-UCNP@pPEG was synthesized and characterized using transmission electron microscopy (TEM), X-ray diffraction (XRD), and Fourier transform infrared (FTIR), among other methods. The loading efficiency of E2 was determined to be 14.5 wt %, and the nanocarrier effectively facilitated sustained release. Confocal upconversion luminescence (UCL) imaging using the CW 980 nm laser as excitation resource revealed significant interactions of E2-UCNP@pPEG with preosteoblasts. E2-UCNP@pPEG treatment of preosteoblasts induced positive effects on differentiation, matrix maturation, and mineralization. Moreover, in situ and ex vivo UCL imaging studies disclosed that E2 encapsulated in the nanocomposite was passively delivered to bone. Our results collectively suggest that this nanoreservoir provides an effective drug-loading system for hormonelike drug delivery and support its considerable potential as a therapeutic agent for osteoporosis.

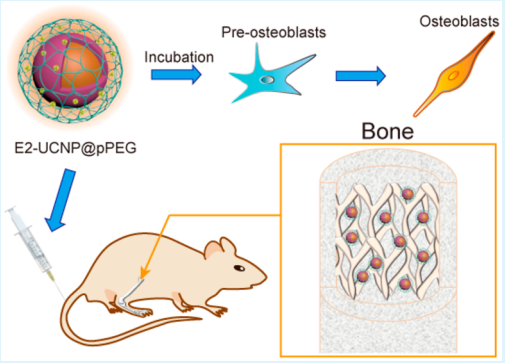

KEYWORDS: *PEGlyated upconversion nanoparticles, 17β-estradiol, drug delivery, imaging, osteoporosis, osteoblast*

1. INTRODUCTION

Osteoporosis is a skeletal disease characterized by low bone mass and microarchitectural deterioration, resulting in increased bone fragility and subsequent susceptibility to fracture.[1] The increasing prevalence of osteoporosis has led to a considerable decline in quality of life in the elderly because of susceptibility to disease-associated fractures.[2] Bone mass is maintained by two phases of bone remodeling, specifically, osteoblast-mediated bone formation and osteoclast-mediated bone resorption, that are normally in dynamic equilibrium. Osteoporosis occurs when the balance collapses, and bone resorption is greater than bone formation.[3] Estrogen induces suppression of osteoclast bone resorption, both in vivo and in vitro,[4] and enhances osteoblast differentiation and bone formation.[5] 17β-estradiol (E2), an estrogen compound, has been shown to inhibit bone resorption, enhance bone formation in tibia and femur in ovariectomized rats,[6] and reinforce proliferation and differentiation of osteoblasts.[7] Accordingly, hormone (estrogen) replacement therapies (HRT) play an important role in the treatment and prevention of osteoporosis.[8] However, studies have shown that long time use of estrogen increases the risk of diseases, such as breast and ovarian cancer, uterine bleeding, and hyperplasia.[9,10] The occurrence of myocardial infarction and cardiovascular disease are also increased.[11] Oral administration is the main method of estrogen intake, but metabolism mainly occurs in the gastrointestinal tract and liver. The plasma concentration of estrogen fluctuates, and high doses are required to achieve the necessary therapeutic effect. Intravenous administration triggers a rapid increase in levels in blood, fast clearance, and pain from the use of injection needles. These potential drawbacks restrict the clinical use of HRT. Therefore, an effective means of improving bioavailability and reducing side-effects are essential for successful application of this therapy.

The use of nanoparticles for drug delivery decreases toxicity and side effects to normal tissues, improves targeting of the drug to given sites, and maintains the activity of hydrophobic drugs.[12,13] Among them, the use of upconversion nanophosphors (UCNPs) as a promising nanocarrier for loading drugs has attracted considerable research attention in recent years. Upconversion luminescence (UCL) is an anti-Stokes procedure that converts low-energy photons into high-energy

Received: April 1, 2015
Accepted: July 2, 2015
Published: July 2, 2015

DOI: 10.1021/acsami.5b02831
ACS Appl. Mater. Interfaces 2015, 7, 15803−15811

photons.[14] On the basis of near-infrared (NIR) excitation in the optimal window for organisms,[15] UCNPs serve as excellent optical trackers for drug delivery with superior properties, such as lack of photodamage for biological tissue,[16] no autofluorescence,[17] no photobleaching,[18] and promotion of penetration depth.[19] Recently, a few groups have demonstrated the rational strategy of UCNP-based drug delivery and monitoring systems,[20−23] and most of them focused on the loading of doxorubicin (DOX) for tumor therapy. To date, no upconversion nanosystem has been reported for osteoporosis therapy application.

Here, we designed and synthesized an E2-loaded upconversion nanosystem (E2-UCNP@pPEG) for bone targeting. Considering that PEGylated nanoparticles possess an excellent stealth effect to mononuclear phagocyte system (MPS) and are more inclined to target bone,[24,25] we coated amphiphilic block-polymer C_{18}PMH-PEG (pPEG, Scheme 1) onto the surface of hydrophobic oleic acid (OA)-coated core−shell upconversion nanocrystal (UCNP) $NaYF_4$:Yb,Er@$NaLuF_4$ to fabricate a hydrophilic nanostructure (UCNP@pPEG) on the basis of the hydrophobic−hydrophobic interaction. Then, hydrophobic E2 was loaded into the hydrophobic layer of UCNP@pPEG to form E2-UCNP@pPEG (Scheme 1). The external PEG chains formed a barrier to retain camouflaging of particles and entrap E2. Biosafety and biological effects of the nanocomposite in preosteoblasts were investigated in vitro. Notably, the newly designed nanosystem had bone-targeting potential, therefore providing an effective model for studying the behavior of nonfluorescent drugs, both in vitro and in vivo.

Scheme 1. Schematic Synthesis Illustration of the Upconversion Nanosystem (E2-UCNP@pPEG)[a]

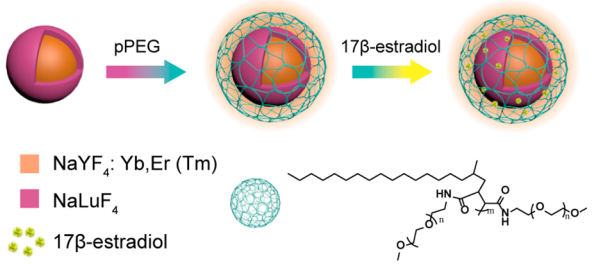

[a]Nanosystem was synthesized by coating an amphiphilic block-polymer C_{18}PMH-PEG (pPEG) on core−shell nanocrystal $NaYF_4$:Yb,Er@$NaLuF_4$ (UCNPs) and then loading 17β-estradiol (E2) into the surface hydrophobic layer.

2. EXPERIMENTAL SECTION

2.1. Materials. Rare-earth oxides (RE_2O_3, 99.999%, RE^{3+} = Y^{3+}, Er^{3+}, Yb^{3+}, and Tm^{3+}) were purchased from Beijing Lansu Co., Ltd. Oleic acid (OA) (>90%), 1-octadecence (ODE) (>90%), and 17β-estradiol (E2) were purchased from Sigma Co., Ltd. NaOH, NH_4F, ethanol, cyclohexane, and hydrochloride solution (37 wt %) were purchased from Sinopharm Chemical Reagent Co., China. Rare-earth chlorides ($RECl_3$, RE^{3+} = Y^{3+}, Lu^{3+}, Yb^{3+}, Er^{3+}, and Tm^{3+}) were prepared by dissolving the corresponding rare-earth oxide in 10 wt % hydrochloride solution at elevated temperature and then evaporating the water completely.[26] All other chemical reagents were analytical-grade and were used directly without further purification. Deionized water was used throughout the experiments. Poly(maleic anhydride-*alt*-1-octadecene)−poly(ethylene glycol) (C_{18}PMH-PEG)[27] was prepared according to the literature.

2.2. Characterization. Powder X-ray diffraction (XRD) measurements were carried out on a Bruker D4 diffractometer (Cu Kα radiation, λ = 1.54056 Å) at a scanning rate of 1°/min in the 2θ range of 10−90°. The size and morphology of UCNPs were determined at 200 kV using a Tecnai G2 20 TWIN low-to-high-resolution transmission electron microscope (TEM). Energy-dispersive X-ray (EDX) analysis and elemental mapping of UCNPs were also recorded during high-resolution TEM (HR-TEM) measurements. The standard TEM samples were prepared by dropping a diluted cyclohexane solution of UCNPs onto the surface of a copper grid. Fourier transform infrared (FTIR) spectra were obtained from samples in KBr pellets using an IRPRESTIGE-21 spectrometer (Shimadzu). Ultraviolet−visible (UV−vis) absorption spectra were recorded on a Shimadzu UV 2550 spectrometer. The upconversion luminescence (UCL) spectra were recorded on Edinburgh FLS-920 instrument using an excitation source of external 0−3 W adjustable 980 nm semiconductor laser (Connet Fiber Optics, China), instead of the xenon source in the spectrophotometer. All the photoluminescence studies were carried out at room temperature.

2.3. Synthesis of Nanomaterials. *2.3.1. Synthesis of $NaYF_4$:Yb,Er (or $NaYF_4$:Yb,Tm) Nanocrystal.* The $NaYF_4$:Yb,Er nanocrystals were prepared by a solvothermal method.[28] In a typical procedure, 1 mmol of $RECl_3$ (RE^{3+} = Y^{3+}, Yb^{3+}, and Er^{3+}) with a molar ratio of 78:20:2 or 1 mmol of $RECl_3$ (RE^{3+} = Y^{3+}, Yb^{3+}, and Tm^{3+}) with a molar ratio of 79:20:1 was added into a mixture of 6 mL of OA and 15 mL of ODE in a three-necked flask (100 mL) at room temperature. Then, the mixture was heated to 140 °C to remove water and oxygen with vigorous magnetic stirring under vacuum for several minutes, forming a clear solution. After cooling to room temperature, 5 mL of methanol solution of NH_4F (4 mmol) and NaOH (2.5 mmol) was slowly added into the flask and stirred for 20 min. After being heated to 100 °C for 20 min to remove the methanol, the solution was heated to 300 °C and maintained for 1 h under a N_2 atmosphere. Upon cooling to room temperature, the nanoparticles were precipitated by adding excess amounts of absolute ethanol into the reacted solution and then collected by centrifugation. After being washed with absolute ethanol and cyclohexane three times, nanoparticles were dispersed in 10 mL of cyclohexane for the next step.

2.3.2. Synthesis of Core−shell Nanocrystals $NaYF_4$:Yb,Er@$NaLuF_4$ (or $NaYF_4$:Yb,Tm@$NaLuF_4$) (UCNP)s. Similarly, $NaYF_4$:Yb,Er@$NaLuF_4$ (or $NaYF_4$:Yb,Tm@$NaLuF_4$) core−shell nanocrystals were synthesized by a modified solvothermal method.[28] The $NaLuF_4$ shell precursor was prepared by dissolving 1 mmol $LuCl_3$ in 6 mL of OA and 15 mL of ODE in a 100 mL flask followed by heating at 140 °C for 30 min. After cooling down to room temperature, $NaYF_4$:Yb,Er (or $NaYF_4$:Yb,Tm) core nanoparticles dispersed in 3 mL of cyclohexane was added dropwise into the solution. Then the mixture was kept at 80 °C for 20 min to remove cyclohexane and cooled to room temperature. Then 5 mL of methanol solution of NH_4F (4 mmol) and NaOH (2.5 mmol) was added. After being heated to 100 °C for 20 min to remove the methanol, the solution was heated to 300 °C and maintained for 1 h under a N_2 atmosphere. Upon cooling to room temperature, the nanoparticles were precipitated by adding an excess amount of absolute ethanol into the reacted solution and then collected by centrifugation. Then the product was washed by absolute ethanol and cyclohexane for three times and dispersed in cyclohexane prior to being used.

2.3.3. Synthesis of UCNP@pPEG. In a typical process, C_{18}PMH-PEG (pPEG, 10 mg) and the core−shell UCNPs (10 mg) were dispersed separately in chloroform (5 mL) and then mixed together and stirred for 2 h to evaporate the chloroform. Then, the rest of the materials were washed with water and dispersed easily in water.[29]

2.4. Loading of 17β-Estradiol (E2) into UCNP@pPEG. E2 (5 mg) dissolved in DMSO (50 μL) was added dropwise into an aqueous solution of UCNP@pPEG. The mixture was then stirred overnight. Free E2 was removed by centrifugation at 15 000 rpm for 10 min. The precipitate was washed with water for three times. The as-obtained precipitate (E2-UCNP@pPEG) was resuspended by a brief sonication to form a homogeneous clear solution.[30] The loading capacity of E2-

DOI: 10.1021/acsami.5b02831
ACS Appl. Mater. Interfaces 2015, 7, 15803−15811

Table 1. Sequences of Primers for RT-PCR

gene	forward primer (5′−3′)	reverse primer (5′−3′)
GAPDH	GGTGAAGGTCGGTGTGAACG	CTCGCTCCTGGAAGATGGTG
OPN	GCTTGGCTTATGGACTGAGG	GGCTTTGGAACTTGCTTGAC
OPG	CCATCTTTCTGCTCACTCTGC	ACGGGATACACACACCCTCT
Col-I	TTCGTGGTTCTCAGGGTAGC	TCCTTGGTTAGGGTCAATCC

UCNP@pPEG was calculated using the UV−vis absorption spectroscopy.

2.5. Release Property of 17β-Estradiol (E2) from E2-UCNP@pPEG. E2-UCNP@pPEG (2 mg/mL) was dispersed in 3 mL of phosphate buffer saline (PBS, pH 7.4) at 37 °C. A small aliquot of the solution was taken at given time intervals, and the concentration of supernatant containing released E2 were determined by UV−vis spectroscopy.[31]

2.6. Cell Culture. Preosteoblasts (a murine calvarial cell line) were purchased from the cell resource center of Shanghai Institutes for Biological Sciences (SIBS). Preosteoblasts were cultured in α-modified minimal essential medium (α-MEM; GIBCO) with 10% fetal bovine serum (FBS), 1% folic acid and inositol, 100 U/mL penicillin, and 100 μg/mL streptomycin. The cells were maintained at 37 °C in a humidified 5% CO_2 atmosphere, and every 2−3 days, the culture medium was changed.

2.7. Viability Assay. The in vitro viability assay was determined using the 3-(4,5-dimethylthiazol-2-yl)-2,5-diphenyltetrazolium bromide (MTT, Sigma-Aldrich, USA) assay. Preosteoblasts were seeded in α-MEM with 10% FBS on 96-well plates. After 24 h, the medium was replaced with phenol-red-free α-MEM containing 5% charcoal-stripped (CS)-FBS (Biological Industries) in the presence of E2-UCNP@pPEG with inner 17β-estradiol (Sigma-Aldrich, USA) at different concentrations (10^{-9}, 10^{-8}, 10^{-7}, and 10^{-6} mol/L); the concentration of the group with 17β-estradiol alone was 10^{-7} mol/L. After completion of the treatment, which was maintained for 1, 3, and 7 days, cells were washed with PBS, and 10 μL of 5 mg/mL MTT was added to the cells and incubated for 4 h at 37 °C. The medium was then removed, and 150 μL of dimethyl sulfoxide was added per well. The plates were kept on a rocker shaker for 15 min at room temperature, and the optical density of each sample was measured with a microplate reader (Biotek, USA) at 570 nm.

2.8. Alkaline Phosphatase Activity and Staining Assay. Preosteoblasts were suspended in α-MEM containing 10% FBS, and plated at a density of 1.5×10^4 cells per well into 24-well chambers. After 24 h, the medium was replaced with phenol-red-free α-MEM containing 5% CS-FBS, 10 mmol/L β-glycerophosphate (β-GP), and 50 μg/L L-ascorbic acid. Cells were cultured with E2 (10^{-7} mol/L), E2-UCNP@pPEG with an inner E2 concentration of 10^{-7} mol/L, or UCNP@pPEG. Each treatment was maintained for 3, 7, and 14 days, with culture medium changes every 2−3 days. After treatment, the medium was removed, and the cell monolayer was gently washed twice with PBS and lysed with 0.2% Triton X-100. Cell lysates were centrifuged at 12 000 g for 10 min, and the clear supernatant was used for measurement of alkaline phosphatase (ALP) activity and protein concentration. ALP activity was determined using an ALP assay kit (Beyotime, Jiangsu, China), and results were normalized to the total intracellular protein content of the sample, which was quantified using the bicinchoninic acid (BCA) protein assay kit (Beyotime), according to the manufacturer's instructions.

For ALP staining, preosteoblasts were seeded into six-well plates at a density of 5×10^4 cells per well. After treatment with E2, UCNP@pPEG, and E2-UCNP@pPEG for 7 days, the medium was removed, and the cell monolayer was gently washed three times with PBS and fixed with 4% paraformaldehyde for 15 min. Cells were stained using the BCIP/NBT alkaline phosphatase staining assay kit (Beyotime), in accordance with the manufacturer's protocol.

2.9. Alizarin Red Staining. Alizarin red staining was used to assess the formation of mineralized matrix nodules. Preosteoblasts were seeded into six-well plates. After 24 h, the medium was replaced with phenol-red-free α-MEM containing 5% CS-FBS, 10 mmol/L β-GP, and 50 μg/L L-ascorbic acid. Adherent cells were treated with E2, UCNP@pPEG, or E2-UCNP@pPEG for a period of 21 days. For staining, cells were fixed with 4% paraformaldehyde for 15 min at room temperature and rinsed twice with PBS (pH 4.2). Cultures were stained with 2% alizarin red (Sigma, USA) for 30 min. Images of stained cells were obtained using a commercial digital camera and light microscopy analysis (Epson Perfection 4990 Photo Scanner, USA).

2.10. Semiquantitative Reverse Transcription-Polymerase Chain Reaction. Total RNA was extracted from preosteoblasts adhered to different substrates after culture for 7 days using the TRIzol Reagent kit (TaKaRa, Otsu, Japan). The reverse transcription reaction for cDNA synthesis was carried out using the cDNA Reverse Transcription Kit (TaKaRa). Four representative genes were selected for analysis. Amplification was carried out using 1 μL of template, 0.1 μL of TaKaRa *Taq*, 2 μL of *Taq* Buffer (10×, Mg^{2+} Plus), 1.6 μL of dNTP mixture, and 0.4 μL of specific primers (20 mol/L) (Table 1) for each cDNA in a total reaction volume of 20 μL. The reaction conditions were as follows: initial denaturation at 94 °C for 1 min, denaturation at 98 °C for 10 s, annealing at 57 °C for 30 s, and final extension at 72 °C for 1 min for osteopontin (OPN). For osteoprotegerin (OPG), the annealing temperature was also 57 °C, and 28 cycles were used. The annealing temperature for type I collagen (Col-I) was 56 °C, and the cycle number was 18. PCR products were analyzed via 2% agarose gel electrophoresis and visualized with GelRed.

2.11. Statistical Analysis. All results are presented as mean ± standard deviation (SD), obtained from experiments repeated at least three times. One-way analysis of variance (ANOVA) or Student's *t* test was used to perform statistical comparisons between groups. Statistical significance was inferred at a probability (P) value of <0.05.

2.12. In Situ and ex Vivo UCL Imaging. Animal procedures were in agreement with the guidelines of the Institutional Animal Care and Use Committee. In situ and ex vivo UCL imaging were carried out with a modified Kodak in vivo imaging system consisting of an external 0−5 W adjustable CW infrared laser (980 nm, Connet Fiber Optics, China) as the excited source and an Andor DU897 EMCCD as the signal collector. UCL signals were collected at 800 ± 12 nm.[32] Images of UCL signals were analyzed with Carestream MI SE. Kunming mice (4 weeks old) were injected intravenously with Tm^{3+}-doped E2-UCNP@pPEG (200 μL, 1.5 mg/mL) in PBS. The control group was injected with PBS (200 μL) via tail vein. At 6 h postinjection, we carried out whole-body imaging without the major organs to expose the bone. After that, bones (arm, leg, sternum, and spine) were removed for ex vivo imaging.

2.13. H&E-Stained Tissues. Kunming mice were intravenously injected with 200 μL of E2-UCNP@pPEG (1.5 mg/mL) and PBS, respectively. At 24 h postinjection, organs (liver, spleen, heart, lung, kidney, and bone) were obtained for hematoxylin and eosin (H&E) staining. The tissues were fixed in paraformaldehyde, embedded in paraffin, sectioned, and stained with H&E. The histological slices were observed under an optical microscope. Moreover, the histological sections of bones were also imaged by confocal microscope.

3. RESULTS AND DISCUSSION

3.1. Synthesis and Characterization of E2-UCNP@pPEG. Intense upconversion luminescence was successfully acquired by developing a core−shell nanocomposite with $NaYF_4$:Yb,Er (or Tm) as the core and $NaLuF_4$ as the shell. The different hosts in core−shell nanocrystals were distinguishable using TEM. $NaYF_4$ core codoped with 20% Yb and 2% Er (or

DOI: 10.1021/acsami.5b02831
ACS Appl. Mater. Interfaces 2015, 7, 15803−15811

1% Tm) was synthesized following a modified solvothermal method. The pure $NaLuF_4$ shell was layered on the surface of $NaYF_4$:Yb,Er via epitaxial growth[28] to obtain $NaYF_4$:Yb,Er@$NaLuF_4$ (or $NaYF_4$:Yb,Tm@$NaLuF_4$) UCNP. Morphological and structural characterization of core−shell nanoparticles was carried out via TEM. The $NaYF_4$:Yb,Er core was spherical with good dispersity and an average size of ∼34 nm, as presented in Figure 1a−c. XRD peaks were well-indexed to hexagonal phase

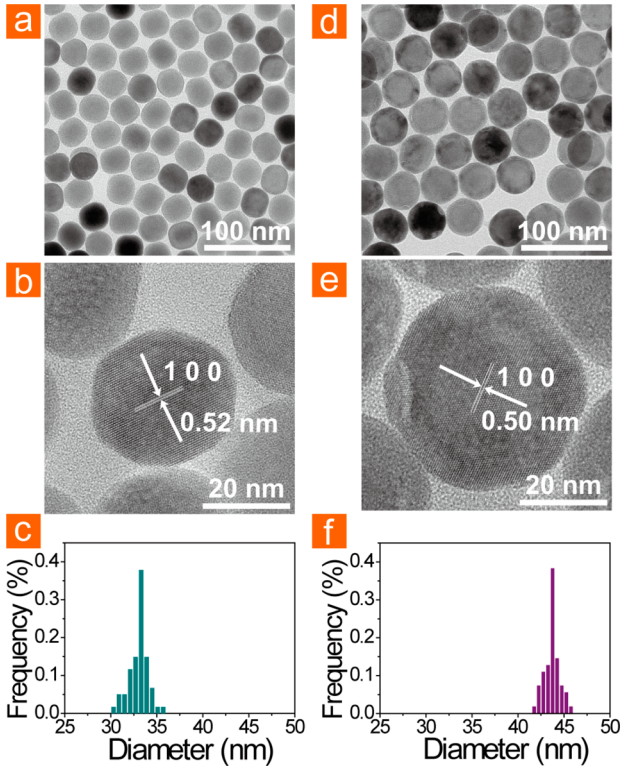

Figure 1. (a) TEM and (b) HR-TEM images of $NaYF_4$:Yb,Er. (c) TEM and (d) HR-TEM images of $NaYF_4$:Yb,Er@$NaLuF_4$. Size distribution of (e) $NaYF_4$:Yb,Er and (f) $NaYF_4$:Yb,Er@$NaLuF_4$.

$NaYF_4$ (Powder Diffraction File (PDF) No.16-0334, International Centre for Diffraction Data (ICDD), [2001]; Figure 2). High crystallinity of nanoparticles was evident, on the basis of distinct lattice fringes in HR-TEM images (Figure 1b). Figure 1 d−f displays the ∼5 nm $NaLuF_4$ shell coated onto the surface of the $NaYF_4$:Yb,Er core. The interplanar spacing of 0.50 nm is in good agreement with d_{100} spacing of hexagonal $NaLuF_4$. EDXA revealed the same elements in $NaYF_4$:Yb,Er@$NaLuF_4$, and $NaYF_4$:Yb,Er, except for the Lu element in $NaYF_4$:Yb,Er@$NaLuF_4$ that displayed a core−shell structure (Figure 2). Scanning TEM (STEM) images (Supporting Information Figure S1) clearly confirmed the different hosts in the $NaYF_4$ core and $NaLuF_4$ shell layers. In addition, element mapping images of Lu and Y provided evidence of $NaLuF_4$ location on the outer layer of $NaYF_4$.

An amphiphilic polymer, C_{18}PMH-PEG (pPEG), was employed to construct a nanocarrier system for loading and release of hydrophobic 17β-estradiol (E2). As illustrated in Scheme 1, oleic acid (OA)-capped UCNP interacts with pPEG through hydrophobic−hydrophobic interactions, thus converting hydrophobic UCNP to a hydrophilic entity with PEG chains on the outside layer. Moreover, the hydrophobic inter layer was used to load E2. The constructure of nanosystem E2-

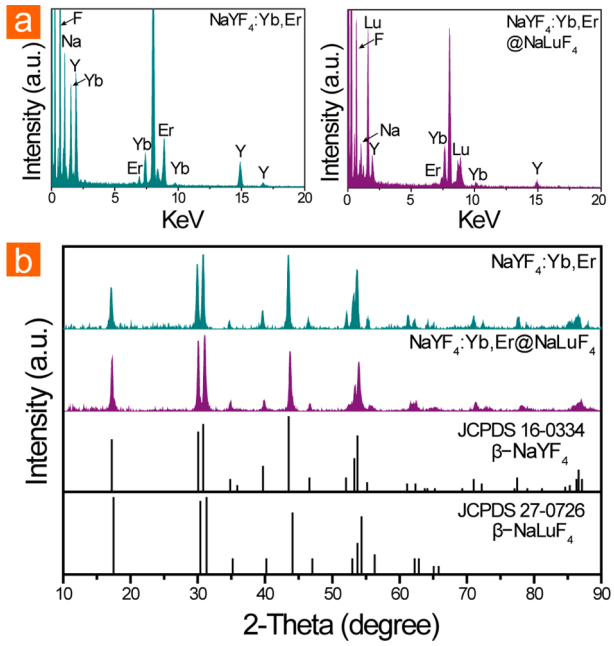

Figure 2. (a) EDXA patterns of $NaYF_4$:Yb,Er and $NaYF_4$:Yb,Er@$NaLuF_4$. (b) XRD patterns of $NaYF_4$:Yb,Er and $NaYF_4$:Yb,Er@$NaLuF_4$ and the standard XRD patterns of β-$NaYF_4$ and β-$NaLuF_4$ (PDF No. 16-0334 and 27-0726, ICCD, [2001]).

UCNP@pPEG was confirmed via FTIR spectroscopy. In the FTIR spectra of UCNP (Supporting Information Figure S4), peaks at 2925 and 2853 cm^{-1} represented asymmetric (as) and symmetric (s) stretching vibrations of long-chain C−H. Peaks at 3008 cm^{-1} represented stretching vibrations of =C−H, indicating that UCNP is modified by oleic acid. In the FTIR spectra of E2-UCNP@pPEG, peaks at 1641 and 1000−1250 cm^{-1} were attributed to C=O and C−O−C stretching vibrations of pPEG, respectively, representing the pPEG coat on UCNP. Bands between 1450 and 1650 cm^{-1} in the spectrum of E2 confirmed the presence of cyclobenzene. Similar IR absorption spectral peaks were observed for E2-UCNP@pPEG, indicative of E2 loading in UCNP@pPEG.

UCL spectra of Er^{3+}-doped UCNP@pPEG and E2-UCNP@pPEG were investigated at room temperature under 980 nm excitation. As shown in Figure 3, UCNP@pPEG in water exhibited three characteristic intense emission bands centered at 520, 540, and 653 nm derived from the $^2H_{11/2} \rightarrow {}^4I_{15/2}$, $^4S_{3/2} \rightarrow {}^4I_{15/2}$, and $^4F_{9/2} \rightarrow {}^4I_{15/2}$ transitions of Er^{3+}, respectively.[17] The intensity of green emission from 515 to 560 nm was similar to the intensity of red emission at 653 nm, resulting in yellow emission visible to the naked eye. Notably, the typical UCL emission spectrum of E2-UCNP@pPEG in water was comparable with that of UCNP@pPEG, except for lower emission strength, but was still sufficiently strong to track E2. Moreover, UCL emission was slightly red after loading E2, probably because of easier quenching of green emission with higher energy (Figure 3, inset). The UCL spectrum of Tm^{3+}-doped E2-UCNP@pPEG is shown in Figure S5 (Supporting Information). Typical emission bands at 450, 475, 646, and 802 nm were assigned to $^1D_2 \rightarrow {}^3F_4$, $^1G_4 \rightarrow {}^3H_6$, $^1G_4 \rightarrow {}^3F_4$, and $^3H_4 \rightarrow {}^3H_6$ transitions of Tm^{3+}, respectively.[33]

Absorption spectra of pure E2 dispersed in dichloromethane contained peaks at 278 and 286 nm (Supporting Information Figure S6). Considering that E2 is released from the

DOI: 10.1021/acsami.5b02831
ACS Appl. Mater. Interfaces 2015, 7, 15803−15811

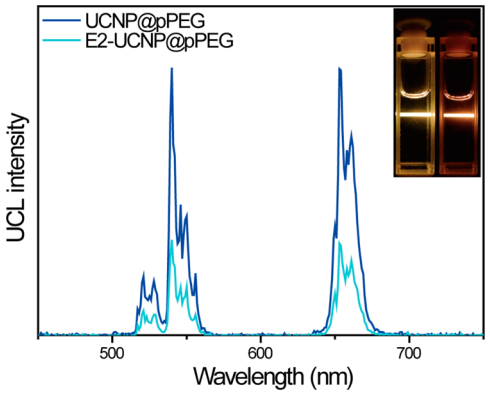

Figure 3. Room-temperature UCL emission spectra of UCNP@pPEG and E2-UCNP@pPEG (doped with Er^{3+}) dispersed in water (2 mg/mL) under excitation at 980 nm (power ≈ 800 mW). Inset: UCL photos of UCNP@pPEG and E2-UCNP@pPEG, from left to right, with a short-pass filter at 720 nm.

nanosystem in organic solvent as pPEG is broken down from the nanosystem, the loading efficiency of E2 was determined using UV−vis absorption spectroscopy.[29] As shown in Figure S7 (Supporting Information), loading efficiency of E2 was calculated to be 14.5 wt %.

Release behavior of E2 from E2-UCNP@pPEG was investigated in PBS solution at pH 7.4 (Figure 4). A rapid

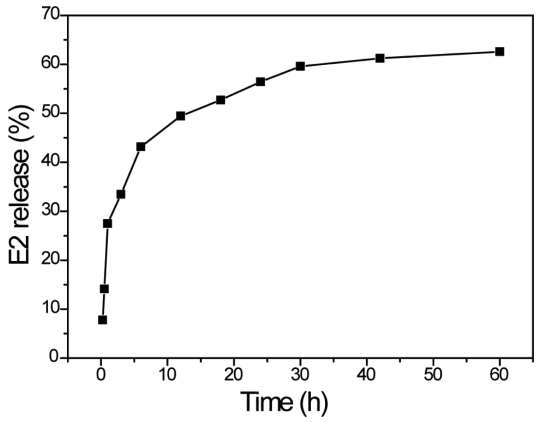

Figure 4. Release behavior of E2 from E2-UCNP@pPEG in PBS solution (pH 7.4).

release rate was observed in 12 h, resulting in delivery of more than 50% of the loading drug. Subsequent release rate was slow, and >60% drug was released after 60 h. It is worth mentioning that under pH 5.0 the release rate of E2 from E2-UCNP@pPEG was similar to that at pH 7.4 which proved that the release behavior of E2 from E2-UCNP@pPEG is not sensitive to pH (Supporting Information Figure S8). The results collectively suggest that this nanosystem can be effectively used as a sustained release carrier for therapeutic hormones.

3.2. Viability Assay of Preosteoblasts Treated with E2-UCNP@pPEG. Measurement of cell viability is the main method used to assess novel drug delivery systems. The MTT assay provides a sensitive means to evaluate osteoblast proliferation because cell viability is measured from determination of dehydrogenase activity in mitochondria. Preosteoblasts were cultured with E2-UCNP@pPEG containing different concentrations of inner E2 (10^{-9}, 10^{-8}, 10^{-7}, and 10^{-6} mol/L) for 1, 3, or 7 days. Our MTT data revealed no significant differences in optical density (OD) values between control and treatment groups at 1, 3, and 7 days ($P > 0.05$, Figure 5). Accordingly, we conclude that E2-UCNP@pPEG is relatively nontoxic to cells.

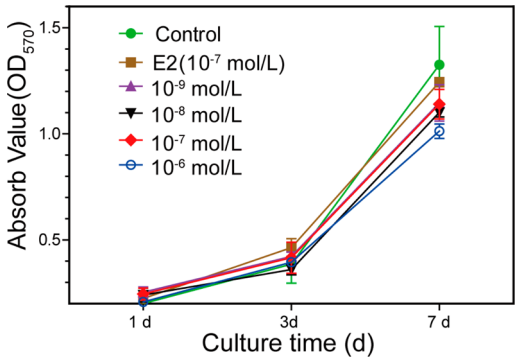

Figure 5. Graph of MTT results for each group at different inner E2 concentrations and treatment durations (mean ± SD). The viability of preosteoblasts was measured by MTT assays after treatment with E2-UCNP@pPEG with inner 17β-estradiol at different concentrations (10^{-9}, 10^{-8}, 10^{-7}, and 10^{-6} mol/L) or 17β-estradiol alone (10^{-7} mol/L). E2 = 17β-estradiol.

3.3. Tracking of E2-UCNP@pPEG in Vitro. An effective nanocarrier should release E2 precisely to minimize its side effects and protect its activity before arrival at the action sites. Therefore, critical interactions of preosteoblasts with nanosystem were determined using laser scanning upconversion luminescence microscopy (LSUCLM). UCL emission of nanocarriers was observed in preosteoblasts after incubation for 3 h at 37 °C under the CW 980 nm laser. Red emission of propidium iodide (PI) staining for fixed cell nuclei was simultaneously observed under 515 nm excitation. As shown in Figure 6, the intensity and location of UCL signals in cells incubated with UCNP@pPEG and E2-UCNP@pPEG were comparable. Overlay of UCL emission, PI signals, and bright field images confirmed that the nanosystem can be successfully taken up by preosteoblasts.

3.4. ALP Activity and Staining Assay of E2-UCNP@pPEG in Preosteoblasts. Osteoblasts express ALP, an important marker of bone differentiation.[4,34] Cells were incubated with E2, E2-UCNP@pPEG, or UCNP@pPEG for 3, 7, and 14 days, and ALP activity was measured. The 7 and 14 day measurements of ALP activity are shown in Figure S9 (Supporting Information) and Figure 7a, respectively. The ALP activity of preosteoblasts achieved its peak when the cells were cultured for 5−7 days. As the incubated period extended, the ALP activity of preosteoblasts tended to decline. These results are consistent with previous reported experiments.[35] The results displayed that treatment with E2, E2-UCNP@pPEG, or UCNP@pPEG led to upregulation of ALP activity compared with that of the control group ($P < 0.01$). Group E2-UCNP@pPEG showed a distinctly higher ALP activity compared to that of the control and UCNP@pPEG group in preosteoblasts after treatment for 14 days. No significant differences were observed between the treatment and control groups on day 3 ($P > 0.05$). ALP staining results were consistent with 7 day ALP activity (Figure 7b). Cells cultured in the presence of E2-UCNP@pPEG displayed increased ALP content and enhanced bone differentiation. Because PEG itself possesses excellent water

DOI: 10.1021/acsami.5b02831
ACS Appl. Mater. Interfaces 2015, 7, 15803−15811

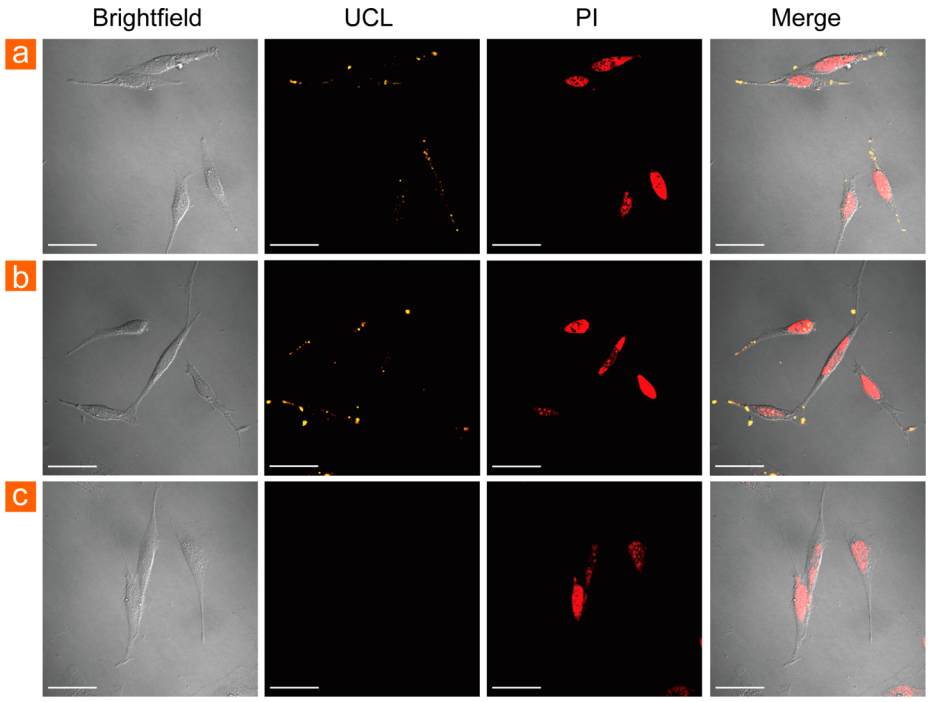

Figure 6. (a) LSUCLM images of fixed preosteoblasts incubated with Er^{3+}-doped E2-UCNP@pPEG (a, 200 μg/mL), UCNP@pPEG (b, 200 μg/mL), or PBS (c, control) for 3 h at 37 °C with CW 980 nm laser. UCL signals were collected from 500 to 560 nm and from 600 to 700 nm, respectively. The nuclei of cells were stained with PI. PI signal was collected from 600 to 650 nm. The scale bar represents 40 μm.

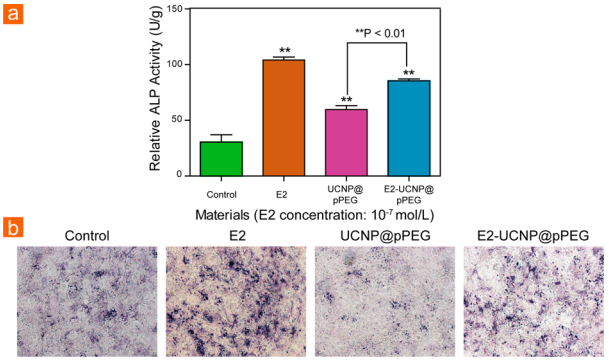

Figure 7. Effects of E2-UCNP@pPEG on (a) ALP activity for 14 days and (b) staining assay in preosteoblasts after treatment for 7 days. The data were represented as the mean ± SD of three determinations. *, $P < 0.05$, and **, $P < 0.01$, compared with the control group.

solubility and biocompatibility, suppresses protein adsorption, and enhances cellular adhesion[36] and E2 itself is hydrophobic and a low dissolved quantity may delay the osteogenesis effects in vitro, UCNP@pPEG displayed favorable cellular growth and differentiation.

3.5. Mineralization Assay. After a period of extracellular matrix maturation, cells begin to mineralize, and calcified nodules developed. Alizarin red staining was applied to confirm the existence of calcium in cellular sediment. Following incubation for 21 days, red-stained mineralized nodules were observed in both experimental and control groups. In the E2-UCNP@pPEG and E2 groups, a higher number of red nodules were observed and mineralization was significantly increased compared to those of the control group (Figure 8). E2-UCNP@pPEG promotes mineralized nodule formation and affects osteoblast differentiation of preosteoblasts.

3.6. Expression of OPN, OPG, and Col-I in Preosteoblasts. Expression of osteogenetic markers was analyzed in preosteoblasts cultured on different substrates for 7 days using RT-PCR. We observed constant mRNA expression of OPN, OPG, and Col-I (Figure 9a). Analysis of the relative mRNA quantity revealed the mRNA expression levels of OPG and Col-I were higher in cells incubated with E2, UCNP@pPEG, and E2-UCNP@pPEG compared with the those of control group (Figure 9b). For OPN, the mRNA expression level was also higher in cells incubated with E2-UCNP@pPEG than that in the control group. Because increased Col-I expression occurs at the early proliferative stage and OPN expression is an early marker of osteoblast differentiation,[37,38] this indicated that E2-UCNP@pPEG had positive effects on the proliferation and differentiation of osteoblasts. Because of the characteristics of PEG itself,[36] UCNP@pPEG displayed the same favorable expression of osteogenetic markers.

3.7. In Situ and ex Vivo UCL Imaging. Kunming mice (4 weeks old) were intravenously injected with Tm^{3+}-doped E2-UCNP@pPEG (200 μL, 1.5 mg/mL) in PBS. After 6 h, whole-body imaging was carried out with a modified Kodak in vivo imaging system using Andor DU897 EMCCD as the signal collector (800 ± 12 nm) upon excitation with an external 0−5 W adjustable CW 980 nm infrared laser. Major organs were removed to expose bone. As shown in Figure 10a, UCL signals were distributed over the whole body, signifying that the E2-UCNP@pPEG was taken up by bone. Subsequently, bone samples from arm, leg, sternum, and spine were removed for ex vivo imaging (Figure 10b). Intense UCL emission was observed, whereas the control group exhibited no obvious signals (Supporting Information Figure S10). UCL images of dissected organs were consistent with the above results. In addition, signals from liver and spleen, the main organs for uptake of nanosized materials, were apparent, although pPEG induced a decrease in accumulation in these regions

DOI: 10.1021/acsami.5b02831
ACS Appl. Mater. Interfaces 2015, 7, 15803−15811

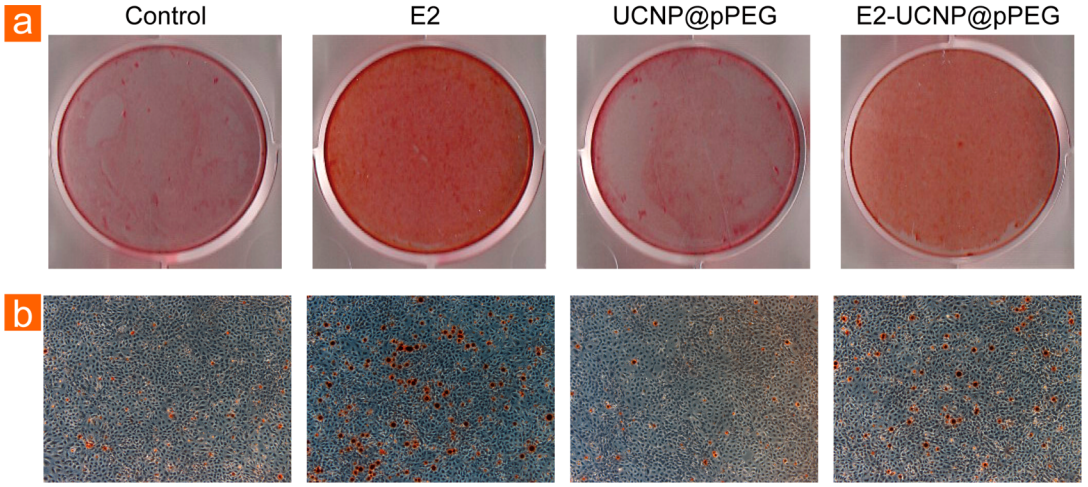

Figure 8. Analysis of E2-UCNP@pPEG to form mineralized nodules of preosteoblasts. Preosteoblasts were stained by Alizarin red. (a) Bright-field photos measured by Nikon camera and (b) their corresponding microscopic images (50×).

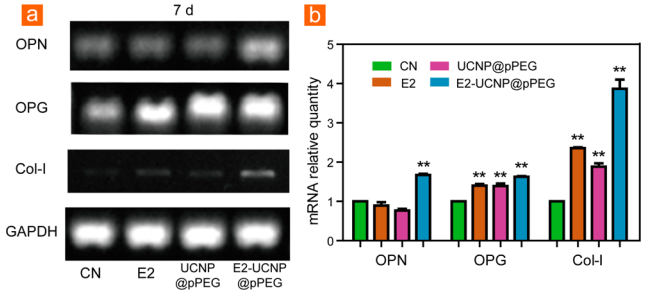

Figure 9. (a) RT-PCR analysis of OPN, OPG, and Col-I expression in preosteoblasts in different substrates cultured for 7 days. GAPDH is the reference gene stably expressed in cells. (b) mRNA relative quantity of OPN, OPG, and Col-I expression in different groups. The concentration of E2 was 10^{-7} mol/L. It showed that the expression level of OPN, OPG, and Col-I was higher in cells incubated with E2-UCNP@pPEG compared with the control group. The data were represented as the mean ± SD of three determinations. **, $P < 0.01$, compared with the control group.

(Supporting Information Figure S11).[39] Tissue distribution of E2-UCNP@pPEG within dissected organs was analyzed via inductively coupled plasma atomic emission spectroscopy (ICP-AES). Quantitative data confirmed distribution of E2-UCNP@pPEG in bone (Supporting Information Figure S12). Our findings clearly show that E2 encapsulated in the nanosystem is efficiently delivered to bone.

3.8. Histology Analysis. Histological evaluation of tissues is critical to determine the efficiency of nanosystem as drug carriers. Confocal imaging of bone tissue sections confirmed extensive distribution of E2-UCNP@pPEG in the bone (Figure 11). Furthermore, H&E-stained tissue sections of liver, spleen, heart, lung, and kidney were used to toxicity analysis. As shown in Figure S13 (Supporting Information), compared with the control groups, no necrosis was observed in any of the tissues examined, suggestive of low nanoparticle-induced toxicity.

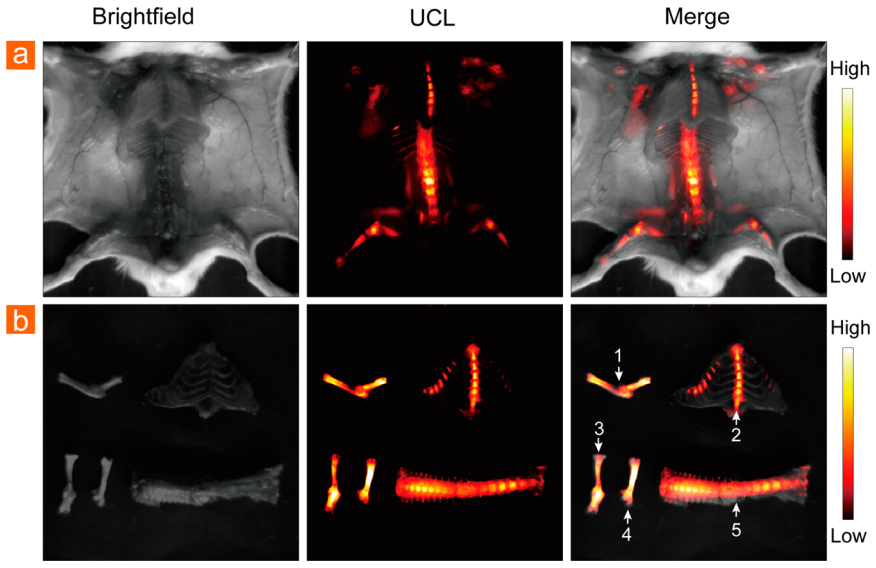

Figure 10. (a) In situ and (b) ex vivo UCL imaging of the Kunming mice 6 h after intravenous injection of 200 μL of Tm^{3+}-doped E2-UCNP@pPEG (1.5 mg/mL). 1, left arm; 2, sternum; 3, left femur; 4, distal left foot; and 5, spine. UCL signals were obtained at 800 ± 12 nm under excitation of CW 980 nm laser.

DOI: 10.1021/acsami.5b02831
ACS Appl. Mater. Interfaces 2015, 7, 15803−15811

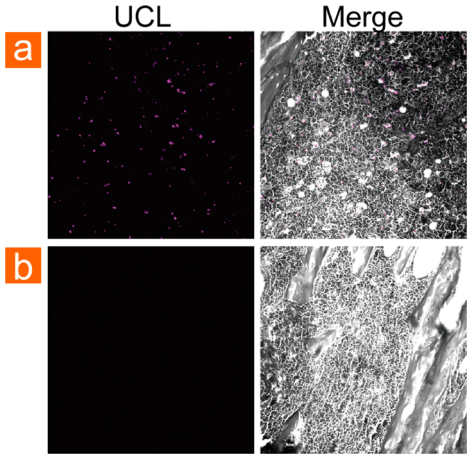

Figure 11. Confocal imaging of bone tissue sections obtained from Kunming mice 24 h after intravenous injection of (a) 200 μL of Tm^{3+}-doped E2-UCNP@pPEG (1.5 mg/mL) and (b) PBS. UCL signals were collected from 420 to 480 nm.

4. CONCLUSIONS

We successfully synthesized E2-loaded PEGylated upconversion nanoparticles (E2-UCNP@pPEG) and analyzed their effects on osteogenesis. PEGylated nanoparticles as a biocompatible nanoreservoir for storing and delivering E2 were generated and characterized. E2 in the fabricated nanocarrier was released in a controlled manner, and the concentration fluctuations were effectively improved. In vitro experiments demonstrated that E2-UCNP@pPEG nanoparticles, as a novel dosage form, modulate bone remodeling and exert a similar biological effect as estrogen alone. In situ and ex vivo imaging data further confirmed the superior bone-targeting ability of E2-UCNP@pPEG. Our results collectively support the utility of the newly generated E2-UCNP@pPEG nanoparticles as an effective therapeutic agent for further osteoporosis. Further studies on osteoclast resorption and in vivo investigation of the efficacy and safety of E2-UCNP@pPEG will be carried out to optimize the utility of these nanoparticles as a therapeutic option for osteoporosis.

■ ASSOCIATED CONTENT

Supporting Information

STEM results of UCNP, TEM results and emission spectrum of UCNP@pPEG, FTIR spectra and loading efficiency of E2-UCNP@pPEG, UV−vis absorption spectrum of E2, UCL imaging of the kunming mice injected with PBS, UCL images of dissected organs injected with or without E2-UCNP@pPEG, biodistribution of E2-UCNP@pPEG in organs, H&E-stained tissue sections from Kunming mice. The Supporting Information is available free of charge on the ACS Publications website at DOI: 10.1021/acsami.5b02831.

■ AUTHOR INFORMATION

Corresponding Authors

*E-mail: yhgao2010@yahoo.com.
*E-mail: fyli@fudan.edu.cn.

Author Contributions

Y.H. and J.L. contributed equally to this work.

Notes

The authors declare no competing financial interest.

■ ACKNOWLEDGMENTS

We thank the State Key Basic Research Program of China (2015CB931800), National Science Foundation of China (81101360 and 21231004), Shanghai Science and Technology Commission (13NM1401101), and the CAS/SAFEA International Partnership Program for Creative Research Teams for financial support.

■ REFERENCES

(1) Poenaru, D. V.; Prejbeanu, R.; Iulian, P.; Haragus, H.; Popovici, E.; Golet, I.; Vermesan, D. Epidemiology of Osteoporotic Hip Fractures in Western Romania. *Int. Orthop.* **2014**, *38*, 2329−2334.
(2) Wang, Y.; Tao, Y.; Hyman, M. E.; Li, J.; Chen, Y. Osteoporosis in China. *Osteoporosis Int.* **2009**, *20*, 1651−1662.
(3) Parfitt, A. M. The Cellular Basis of Bone Remodeling: the Quantum Concept Reexamined in Light of Recent Advances in the Cell Biology of Bone. *Calcif. Tissue Int.* **1984**, *36*, S37−45.
(4) Rickard, D. J.; Subramaniam, M.; Spelsberg, T. C. Molecular and Cellular Mechanisms of Estrogen Action on the Skeleton. *J. Cell. Biochem.* **1999**, *75*, 123−132.
(5) Qu, Q.; Perala-Heape, M.; Kapanen, A.; Dahllund, J.; Salo, J.; Vaananen, H. K.; Harkonen, P. Estrogen Enhances Differentiation of Osteoblasts in Mouse Bone Marrow Culture. *Bone* **1998**, *22*, 201−209.
(6) Tomkinson, A.; Reeve, J.; Shaw, R. W.; Noble, B. S. The Death of Osteocytes via Apoptosis Accompanies Estrogen Withdrawal in Human Bone. *J. Clin. Endocrinol. Metab.* **1997**, *82*, 3128−3135.
(7) Riggs, B. L.; Melton, L. J., 3rd Bone Turnover Matters: the Raloxifene Treatment Paradox of Dramatic Decreases in Vertebral Fractures without Commensurate Increases in Bone Density. *J. Bone Miner. Res.* **2002**, *17*, 11−14.
(8) Hofbauer, L. C.; Khosla, S.; Dunstan, C. R.; Lacey, D. L.; Spelsberg, T. C.; Riggs, B. L. Estrogen Stimulates Gene Expression and Protein Production of Osteoprotegerin in Human Osteoblastic Cells. *Endocrinology* **1999**, *140*, 4367−4370.
(9) Gray, S. Breast Cancer and Hormone-Replacement Therapy: the Million Women Study. *Lancet* **2003**, *362*, 1332.
(10) Lacey, J. V., Jr.; Mink, P. J.; Lubin, J. H.; Sherman, M. E.; Troisi, R.; Hartge, P.; Schatzkin, A.; Schairer, C. Menopausal Hormone Replacement Therapy and Risk of Ovarian Cancer. *Jama* **2002**, *288*, 334−341.
(11) Mueck, A. O. Postmenopausal Hormone Replacement Therapy and Cardiovascular Disease: the Value of Transdermal Estradiol and Micronized Progesterone. *Climacteric* **2012**, *15*, 11−17.
(12) Farokhzad, O. C.; Langer, R. Impact of Nanotechnology on Drug Delivery. *ACS Nano* **2009**, *3*, 16−20.
(13) Mura, S.; Nicolas, J.; Couvreur, P. Stimuli-Responsive Nanocarriers for Drug Delivery. *Nat. Mater.* **2013**, *12*, 991−1003.
(14) Zhou, J.; Liu, Z.; Li, F. Y. Upconversion Nanophosphors for Small-Animal Imaging. *Chem. Soc. Rev.* **2012**, *41*, 1323−1349.
(15) Welsher, K.; Liu, Z.; Sherlock, S. P.; Robinson, J. T.; Chen, Z.; Daranciang, D.; Dai, H. J. A Route to Brightly Fluorescent Carbon Nanotubes for Near-Infrared Imaging in Mice. *Nat. Nanotechnol.* **2009**, *4*, 773−780.
(16) Zhou, J.; Liu, Q.; Feng, W.; Sun, Y.; Li, F. Y. Upconversion Luminescence Materials: Advances and Applications. *Chem. Rev.* **2015**, *115*, 395−465.
(17) Yu, M. X.; Li, F. Y.; Chen, Z. G.; Hu, H.; Zhan, C.; Yang, H.; Huang, C. H. Laser Scanning Up-Conversion Luminescence Microscopy for Imaging Cells Labeled with Rare-Earth Nanophosphors. *Anal. Chem.* **2009**, *81*, 930−935.
(18) Chen, G. Y.; Ohulchanskyy, T. Y.; Kumar, R.; Agren, H.; Prasad, P. N. Ultrasmall Monodisperse $NaYF_4$:Yb^{3+}/Tm^{3+} Nanocrystals with Enhanced Near-Infrared to Near-Infrared Upconversion Photoluminescence. *ACS Nano* **2010**, *4*, 3163−3168.
(19) Wang, F.; Banerjee, D.; Liu, Y. S.; Chen, X. Y.; Liu, X. G. Upconversion Nanoparticles in Biological Labeling, Imaging, and Therapy. *Analyst* **2010**, *135*, 1839−1854.

DOI: 10.1021/acsami.5b02831
ACS Appl. Mater. Interfaces 2015, 7, 15803−15811

(20) Liu, J. N.; Bu, J. W.; Bu, W. B.; Zhang, S. J.; Pan, L. M.; Fan, W. P.; Chen, F.; Zhou, L. P.; Peng, W. J.; Zhao, K. L.; Zhao, K. L.; Du, J. L.; Shi, J. L. Real-Time *in Vivo* Quantitative Monitoring of Drug Release by Dual-Mode Magnetic Resonance and Upconverted Luminescence Imaging. *Angew. Chem., Int. Ed.* **2014**, *53*, 4551−4555.
(21) Hou, Z. Y.; Li, X. J.; Li, C. X.; Dai, Y. L.; Ma, P. A.; Zhang, X.; Kang, X. J.; Cheng, Z. Y.; Lin, J. Electrospun Upconversion Composite Fibers as Dual Drugs Delivery System with Individual Release Properties. *Langmuir* **2013**, *29*, 9473−9482.
(22) Dai, Y. L.; Yang, D. M.; Kang, X. J.; Zhang, X.; Li, C. X.; Hou, Z. Y.; Cheng, Z. Y.; Lin, J. Doxorubicin Conjugated $NaYF_4$: Yb^{3+}/Tm^{3+} Nanoparticles for Therapy and Sensing of Drug Delivery by Luminescence Resonance Energy Transfer. *Biomaterials* **2012**, *33*, 8704−8713.
(23) Guo, H. C.; Idris, N. M.; Zhang, Y. LRET-Based Biodetection of DNA Release in Live Cells Using Surface-Modified Upconverting Fluorescent Nanoparticles. *Langmuir* **2011**, *27*, 2854−2860.
(24) Porter, C. J.; Moghimi, S. M.; Illum, L.; Davis, S. S. The Polyoxyethylene/Polyoxypropylene Block Co-polymer Poloxamer-407 Selectively Redirects Intravenously Injected Microspheres to Sinusoidal Endothelial Cells of Rabbit Bone Marrow. *FEBS Lett.* **1992**, *305*, 62−66.
(25) Moghimi, S. M.; Hedeman, H.; Muir, I.; Illum, L.; Davis, S. S. An Investigation of the Filtration Capacity and the Fate of Large Filtered Sterically-Stabilized Microspheres in Rat Spleen. *Biochim. Biophys. Acta, Gen. Subj.* **1993**, *1157*, 233−240.
(26) Zhu, X. J.; Da Silva, B.; Zou, X. M.; Shen, B.; Sun, Y.; Feng, W.; Li, F. Y. Intra-Arterial Infusion of PEGylated Upconversion Nanophosphors to Improve the Initial Uptake by Tumors in Vivo. *RSC Adv.* **2014**, *4*, 23580−23584.
(27) Prencipe, G.; Tabakman, S. M.; Welsher, K.; Liu, Z.; Goodwin, A. P.; Zhang, L.; Henry, J.; Dai, H. J. PEG Branched Polymer for Functionalization of Nanomaterials with Ultralong Blood Circulation. *J. Am. Chem. Soc.* **2009**, *131*, 4783−4787.
(28) Wang, F.; Deng, R. R.; Wang, J.; Wang, Q. X.; Han, Y.; Zhu, H. M.; Chen, X. Y.; Liu, X. G. Tuning Upconversion through Energy Migration in Core−Shell Nanoparticles. *Nat. Mater.* **2011**, *10*, 968−973.
(29) Yao, L. M.; Zhou, J.; Liu, J. L.; Feng, W.; Li, F. Y. Iridium-Complex-Modified Upconversion Nanophosphors for Effective LRET Detection of Cyanide Anions in Pure Water. *Adv. Funct. Mater.* **2012**, *22*, 2667−2672.
(30) Wang, C.; Cheng, L.; Liu, Z. Drug Delivery with Upconversion Nanoparticles for Multi-Functional Targeted Cancer Cell Imaging and Therapy. *Biomaterials* **2011**, *32*, 1110−1120.
(31) Yang, D. M.; Kang, X. J.; Ma, P. A.; Dai, Y. L.; Hou, Z. Y.; Cheng, Z. Y.; Li, C. X.; Lin, J. Hollow Structured Upconversion Luminescent $NaYF_4$:Yb^{3+},Er^{3+} Nanospheres for Cell Imaging and Targeted Anti-Cancer Drug Delivery. *Biomaterials* **2013**, *34*, 1601−1612.
(32) Liu, Q.; Feng, W.; Yang, T. S.; Yi, T.; Li, F. Y. Upconversion Luminescence Imaging of Cells and Small Animals. *Nat. Protoc.* **2013**, *8*, 2033−2044.
(33) Wang, F.; Wang, J.; Liu, X. G. Direct Evidence of a Surface Quenching Effect on Size-Dependent Luminescence of Upconversion Nanoparticles. *Angew. Chem., Int. Ed.* **2010**, *49*, 7456−7460.
(34) Kim, H.; Tabata, A.; Tomoyasu, T.; Ueno, T.; Uchiyama, S.; Yuasa, K.; Tsuji, A.; Nagamune, H. Estrogen Stimuli Promote Osteoblastic Differentiation via the Subtilisin-Like Proprotein Convertase PACE4 in MC3T3-E1 Cells. *J. Bone Miner. Metab.* **2015**, *33*, 30−39.
(35) Shang, Z. Z.; Li, X.; Sun, H. Q.; Xiao, G. N.; Wang, C. W.; Gong, Q. Differentially Expressed Genes and Signalling Pathways are Involved in Mouse Osteoblast-Like MC3T3-E1 Cells Exposed to 17β-Estradiol. *Int. J. Oral Sci.* **2014**, *6*, 142−149.
(36) Tessmar, J. K.; Gopferich, A. M. Customized PEG-Derived Copolymers for Tissue-Engineering Applications. *Macromol. Biosci.* **2007**, *7*, 23−39.
(37) Zhou, S.; Zilberman, Y.; Wassermann, K.; Bain, S. D.; Sadovsky, Y.; Gazit, D. Estrogen Modulates Estrogen Receptor Alpha and Beta Expression, Osteogenic Activity, and Apoptosis in Mesenchymal Stem Cells (MSCs) of Osteoporotic Mice. *J. Cell. Biochem.* **2001**, *81*, 144−155.
(38) Boyce, B. F.; Xing, L. Functions of RANKL/RANK/OPG in Bone Modeling and Remodeling. *Arch. Biochem. Biophys.* **2008**, *473*, 139−146.
(39) Jokerst, J. V.; Lobovkina, T.; Zare, R. N.; Gambhir, S. S. Nanoparticle PEGylation for Imaging and Therapy. *Nanomedicine* **2011**, *6*, 715−728.

DOI: 10.1021/acsami.5b02831
ACS Appl. Mater. Interfaces 2015, 7, 15803−15811